Structures 51 (2023) 1219–1229

Contents lists available at ScienceDirect

Structures

journal homepage: www.elsevier.com/locate/structures

Experimental and analytical study on structural performance of reinforced lightweight geopolymer composites panels

Zhixing Li, Wensu Chen *, Hong Hao *, Cheng Xu, Thong M. Pham

Centre for Infrastructural Monitoring and Protection, School of Civil and Mechanical Engineering, Curtin University, Australia

ARTICLE INFO

Keywords:
Prefabricated construction
Expanded polystyrene (EPS)
Lightweight geopolymer composite (LGC) panel
Structural performance

ABSTRACT

Various lightweight panels such as autoclaved aerated concrete (AAC) panels have been widely used in the prefabricated construction. With the growing demand for eco-friendly building materials, geopolymer as cementitious material has been extensively studied. A novel ambient-cured lightweight geopolymer composite (LGC) with expanded polystyrene (EPS) was recently developed by the authors and demonstrated sound static and dynamic mechanical properties. In this study, a new lightweight reinforced panel made of LGC is proposed for prefabricated structures. Five full-scale panels, including one AAC panel and four LGC panels with different configurations, were prepared and tested under four-point bending to investigate the effects of panel thickness and reinforcement configuration on the structural performance. The test results showed that the LGC panels demonstrated better structural performance, with the characteristic ultimate bending capacity 57%-110% higher than that of the corresponding AAC panel. An analytical study was also conducted, and empirical formulae were proposed to predict the ultimate bending capacity of LGC panels.

1. Introduction

With the increase in the demand for new construction, the production of concrete increases vastly around the world. The construction industry accounts for about 36% of global energy consumption and is responsible for a great amount of greenhouse gas emissions [1,2]. Ordinary Portland cement (OPC) has been used as the main binder material of conventional concrete and its demand continues to increase at a rate of 9% per year [3]. During OPC production, a massive amount of carbon dioxide (CO_2) is released by calcining non-renewable natural resources, e.g., limestone and gypsum. The amount of CO_2 generated in the OPC manufacturing process accounts for 5–7% of the total emission, which contributes significantly to global warming. [4]. There is a growing demand to find an environmentally friendly alternative to OPC. Moreover, to mitigate the adverse environmental and social effects of traditional construction, the prefabricated construction technology has been increasingly adopted around the world as a sustainable construction method due to its many advantages, such as reduced energy consumption, improved building quality, lower overall construction costs and less construction time [5,6]. The prefabricated construction as one of the advanced construction methods can combine with new green construction materials and less energy-intensive technologies to further reduce greenhouse gas emissions for environmental protection. There is a growing demand for using new lightweight sustainable materials with high strength and other features, e.g., thermal insulation, sound absorption and fire resistance, etc. in prefabrication constructions [7].

The lightweight panels, e.g., reinforced autoclaved aerated concrete (AAC) panels, have been used in domestic and industrial construction [8]. Most previous studies focused on the flexural behaviour of AAC panels with the thickness of 100–300 mm [9–13]. Very limited studies investigated the flexural behaviour of 50 mm-thick AAC panel, although it can be used in panel systems including external walls, partition walls and flooring as per AS 5146 [49], as shown in Fig. 1. Jennings, Owen [14] and Wilson, Jennings [15] studied the performance of 50 mm-thick AAC panels as the floor or cladding panel subjected to transverse gravity loading and uniformly distributed load, respectively. However, AAC is manufactured by using OPC, which could lead to a huge disturbance to natural sources as well as release a massive amount of CO_2 during its calcination [16]. High embodied energy and cost are associated with manufacturing AAC products as it requires high curing temperature, pressure and long curing time [17]. The shortcomings of AAC prefabricated elements were reported, i.e., the high porosity of AAC matrix (i.e., 65–90%), low strength and high water-absorption properties of AAC panel might lead to cracks and breakages as reported in [18].

* Corresponding authors.
E-mail addresses: wensu.chen@curtin.edu.au (W. Chen), hong.hao@curtin.edu.au (H. Hao).

https://doi.org/10.1016/j.istruc.2023.03.129
Received 12 December 2022; Received in revised form 17 March 2023; Accepted 22 March 2023
Available online 28 March 2023

Fig. 1. 50 mm-thick reinforced AAC panel: (a) flooring panel [19] and (b) cladding panel [20].

Therefore, alternative sustainable building materials with sound mechanical properties are highly sought to reduce CO_2 emissions and energy consumption.

In the last two decades, geopolymer as an eco-friendly cementitious material has been extensively studied. With the use of industrial by-products or wastes, such as fly ash and blast furnace slag, geopolymer can reduce greenhouse gas emissions by up to 80% [21]. It is worth mentioning that industrial by-products can result in environmental issues, which has been exacerbated due to global urbanization and industrialization [22]. The use of by-products as raw materials of geopolymer in the construction industry can lessen the pressure on the surrounding environment. Therefore, geopolymer as substitute materials for OPC provides a cost-effective and sustainable solution for both construction and waste management sectors. In recent years, ambient-cured geopolymer was synthesized and intensively investigated [23–26]. As compared to AAC, the ambient-cured geopolymer consumes less energy for fabricating and curing with better durability performance [16,27]. Meanwhile, expanded polystyrene (EPS) is a non-biodegradable and non-photolysis material, which is commonly utilized in packaging, industrial and construction applications [28]. EPS can remain in the soil for hundreds of years and cause severe ecological impact and environmental problems. The over-exploitation of natural resources involved in construction material can be diminished by using EPS as a lightweight aggregate substitute [29]. Therefore, the use of industrial by-products and waste such as fly ash, slag, and EPS as raw materials in lightweight geopolymer composites (LGC) offers a more cost-effective and eco-friendly option compared to AAC, which uses cement and lime as raw materials. Although the economic impact of using LGC in construction is not evaluated as it is beyond the scope of this study, direct and indirect economic benefits, as well as the positive environmental impact are expected through recycling industry and living wastes as construction materials.

LGC with EPS have been produced for non-structural or structural purposes due to their sound properties such as reasonable strength, superior thermal insulation and sound acoustic insulation [27,30–33]. For example, Kakali, Kioupis [30] reported that the thermal conductivity of LGC with the density of 1050 kg/m^3 was 0.16 W/m K, which was similar to that of AAC with the density of 600–700 kg/m^3 (i.e., 0.15–0.18 W/m K) as reported in [34]. Furthermore, EPS concrete was effective in improving the energy absorption capacity [35]. When EPS was subjected to dynamic loading, the entrapped air within the EPS cells was compressed, and viscous force was generated, which could enhance the strain rate sensitivity of LGC with EPS due to the increased viscous forces with the rising loading rate [36,37]. Most of the previous studies investigated EPS concrete as a fill material in sandwich panels [38–41]. It was reported that EPS concrete-based sandwich panels can be used as wall panels. The mechanical performance of sandwich panels is greatly affected by the material of the face sheet and the bonding. Currently, there are very limited studies on the structural behaviour of reinforced EPS concrete panels. Nguyen, Han [42] studied the flexural behaviour of 100 mm-thick lightweight reinforced EPS concrete panels. As reported, the reinforced lightweight panel can be used as structural component in engineering applications. In the previous studies, the authors developed a new ambient-cured LGC with 30% EPS in volume percentages and demonstrated its sound static and dynamic properties [37,43]. The structural performance of lightweight panels made of LGC is worth investigating for engineering applications.

This study developed lightweight panels by using LGC with EPS as an eco-friendly material for sustainable prefabricated building, and their structural performance was investigated and compared with OPC-based AAC panels. The mechanical properties of AAC and LGC were compared first. The structural performance of full-scale AAC and LGC panels with different configurations was experimentally investigated and the Digital Image Correlation (DIC) method was used to monitor the displacement and strain distribution during the tests. The failure modes and the load-carrying capacity of LGC panels were discussed. The empirical formulae for predicting the flexural behaviour of the LGC panel were also proposed, and its prediction was compared with the experimental results.

2. Experimental program

2.1. Design of reinforced panels

A total of five lightweight reinforced panels including one AAC panel (namely AAC_T50L) and four LGC panels (namely LGC_T50L_1, LGC_T50L_2, LGC_T50S and LGC_T37L) were prepared to investigate the flexural behavior under four-point bending tests. Fig. 2 shows the dimension and configuration of the panels. The full-scale panel AAC_T50L had the dimension of 2200-mm in length, 600-mm in width and 50-mm in thickness. One layer of 3.2 mm-diameter steel mesh placed in the mid in AAC_T50L consisted of 12 steel wires in the transverse direction and 4 steel wires in the longitudinal direction as shown in Fig. 2. Two LGC_T50L panels (i.e., LGC_T50L_1 and LGC_T50L_2) were constructed with the same dimension and reinforcement configuration as AAC_T50L to investigate the effect of using LGC on the performance. LGC_T50S had the same dimension as AAC_T50L but used the 2.5-mm-diameter steel mesh with smaller mesh grids, which consisted of 21 steel wires in the transverse direction and 6 steel wires in the longitudinal direction to maintain the same reinforcement ratio (i.e., 0.11 %) as AAC_T50L. It is noted that using smaller mesh grid size is beneficial to resist windborne debris impact on the panel. More number of closely spaced reinforcements with smaller diameter were effective in enhancing perforation resistance and mitigating damage than using less number larger reinforcements with the same reinforcement ratio as

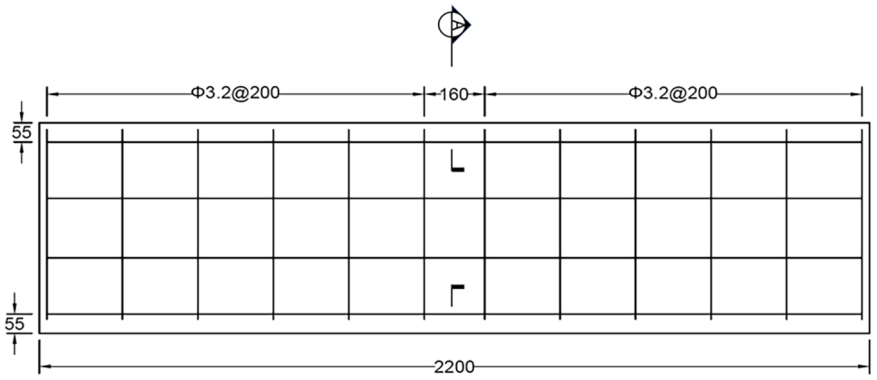

AAC_T50L, LGC_T50L and LGC_T37L

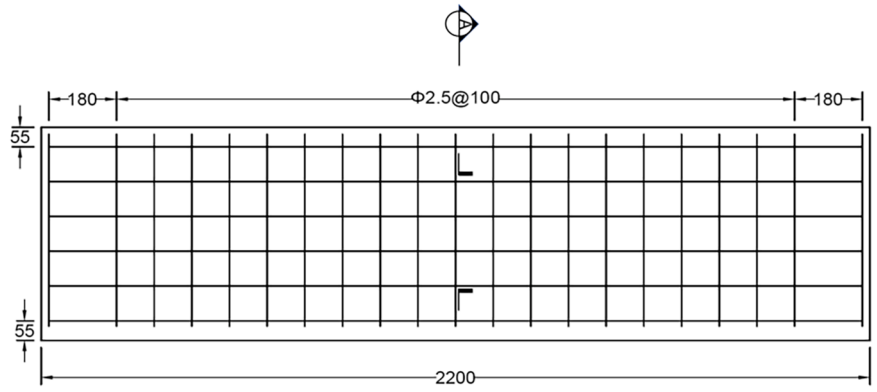

LGC_T50S
(a) Plan View

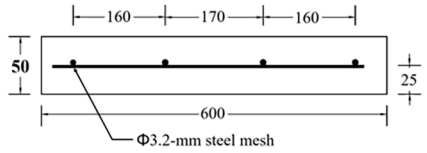

AAC_T50L and LGC_T50L

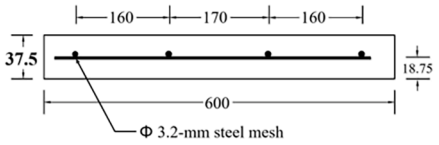

LGC_T37L

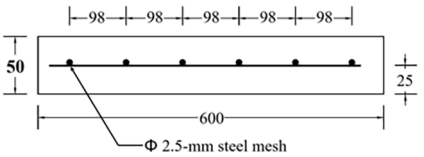

LGC_T50S
(b) Section A-A

Fig. 2. Schematic diagram of the panels (unit: mm) (a) plan view and (b) sectional view.

Table 1
Description of testing specimens.

ID	Matrix material	Density (kg/m^3)	Weight (kg)	Thickness (mm)	Reinforcements (mm)	Reinforcements ratio (%)
AAC_T50L	AAC	765	46.2	50.8	Ø 3.2	0.11
LGC_T50L_1	LGC	1033	71.9	51.5	Ø 3.2	0.11
LGC_T50L_2	LGC	1033	72.3	51.8	Ø 3.2	0.11
LGC_T50S	LGC	1033	73.8	50.4	Ø 2.5	0.11
LGC_T37L	LGC	1033	47.0	37.9	Ø 3.2	0.11

Table 2
Mix proportion of LGC [43].

Constituent	Fly ash	Slag	NaOH	Na_2SiO_3	Sand	EPS
Weight (kg/m^3)	595	105	80	200	325	4

reported in [44]. A smaller grid size can ensure the impact is on the steel mesh and prevent penetration of the panel. Additionally, distributing the impact load evenly over the panel surface can also prevent localized damage and reduce the chances of panel failure. LGC_T37L with 37.5-mm in thickness having a similar weight as AAC_T50L was prepared to compare the structural performance of AAC and LGC panels with the same weight. The ambient density of AAC and LGC was tested before the flexural test as per AS 5146.2 [45]. The configurations of AAC and LGC panels are detailed in Table 1.

2.2. Specimen preparation

In this study, the reinforced AAC panel was provided by a local supplier, Westgyp [46]. The mix design of the LGC with 30% EPS in volume proposed in the authors' previous study [43] was adopted to fabricate lightweight reinforced panels, as shown in Table 2. Low calcium fly ash was provided by Cement Australia from the Gladstone power station, which was classified as class F as per ASTM C618-19 [47]. Ground granulated blast-furnace slag (GGBFS) was sourced from BGC cement. Fly ash and GGBFS at mass ratio of 5.6 were used as binder materials. The chemical compositions of binder material evaluated by X-ray fluorescence analysis are presented in Table 3. Silica sand as fine aggregates was supplied by Hanson Construction Materials. The mass ratio of sand to binder was 0.46. D-grade sodium silicate (Na_2SiO_3) (specific gravity = 1.53) and 8-M (molarity = 8 mol/L) sodium hydroxide (NaOH) solution were combined in mass ratio of 2.5 to activate the geopolymerization reaction. The mass ratio of alkaline activator to binder was determined as 0.4.

The manufacturing process of LGC with EPS is based on the authors' previous study [43] as detailed in Fig. 3. The dry ingredients, including fly ash, slag and sand, were mixed for three minutes, and subsequently, the alkaline activator solution was gradually added into the mixer to obtain geopolymer mortar. Then, EPS beads were blended with the geopolymer mortar for another three minutes to ensure uniform

Table 3
Chemical compositions of slag and fly ash [43].

Composition (wt.%)	SiO_2	Al_2O_3	Fe_2O_3	CaO	MgO	TiO_2	P_2O_5	Na_2O	K_2O	SO_3	MnO	Others	LOI
Slag	32.50	13.56	0.85	41.20	5.10	0.49	0.03	0.27	0.35	3.20	0.25	1.12	1.11
Fly ash	51.10	25.56	12.48	4.30	1.45	1.32	0.88	0.77	0.70	0.25	0.15	0.46	0.57

Note: LOI = loss on ignition.

Fig. 3. Manufacturing process of LGC panels.

Fig. 4. Cross-section of the panels with various thicknesses.

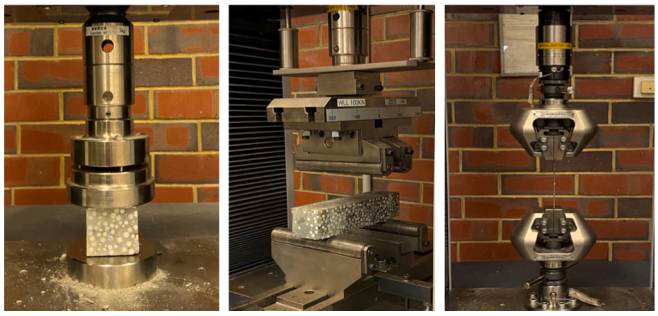

(a) (b) (c)

Fig. 5. Test set-up for (a) compressive test for LGC, (b) flexural test for LGC and (c) tensile test for steel wire.

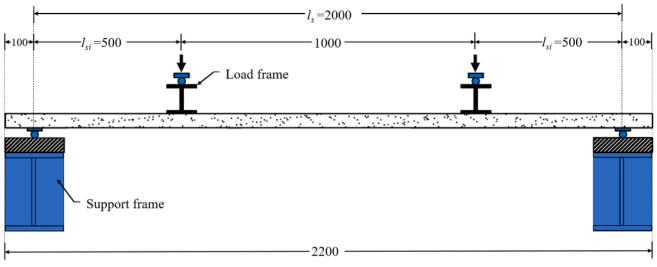

(a)

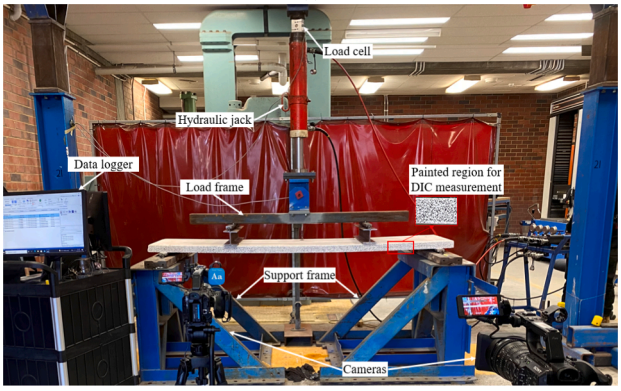

(b)

Fig. 6. Four-point bending test setup: (a) schematic diagram and (b) photograph (unit: mm).

distribution. The resultant LGC mixture was then poured into moulds and subjected to vibration to eliminate trapped air bubbles. After 24 h, the specimens were removed from the moulds and allowed to cure under ambient conditions for 28 days. The cross-sections of LGC panels with various thicknesses in Fig. 4 demonstrate that uniform distribution of EPS beads was achieved.

2.3. Instrumentation and test setup

2.3.1. Material test

The material tests, i.e., compressive and flexural tests for LGC and tensile tests for steel wire, were conducted by using the SHIMADZU testing system, as shown in Fig. 5. A total of 16 cubic specimens with the dimension of 50 × 50 × 50 mm^3 were tested with an equivalent loading rate of 0.33 MPa/min to obtain the compressive strength of LGC at 28 days as per AS 5146.2 [45]. A total of four specimens with the dimensions of 150 × 50 × 50 mm^3 (length × width × height) were tested under an equivalent loading rate of 0.01 mm/s for flexural tests as per AS 5146.2 [45]. The modulus of rupture can be calculated as follows:

Table 4
Material properties of AAC [46] and LGC.

Material	ρ (SD) (kg/m^3)	f_c'(SD) (MPa)	f_r (SD) (MPa)	E (SD) (GPa)
AAC	765 (20.08)	4.18 (0.33)	0.50 (0.08)	1.18 (0.10)
LGC	1033 (28.5)	12.75 (1.4)	1.02 (0.12)	4.83 (0.03)

Note: ρ = density; f_c' = compressive strength; f_r = modulus of rupture; E = modulus of elasticity; and SD = standard deviation.

$$f_{cfi} = F_i l_i / (b_{fri} h_{fri}^2) \quad (1)$$

where f_{cfi} is the modulus of rupture; F_i is the measured breaking load; l_i is the measured distance between the supports; b_{fri} is the width of the specimen at the position of the break; and h_{fri} is the height of the specimen. With respect to the steel mesh of LGC panels, three steel wire coupons for each diameter were tested to obtain the mechanical properties as per AS 4671 [48].

2.3.2. Four-point bending test

Figs. 6 (a) and (b) illustrate the schematic diagram and laboratory setup of four-point bending tests as per AS 5146.2 [45], including a load cell, hydraulic jack, linear variable differential transformer (LVDT), data acquisition system, load frame and support frame. The load was applied via a hydraulic jack with an equivalent rate of 1 mm/min. The load frame, including two 10 kg I-section beams with the dimension of 100 mm × 100 mm × 700 mm (width × height × length) shown in Fig. 6, was used to apply uniform loading across the width of panel. The total applied load is the sum of the applied load provided by the hydraulic jack and self-weight of the load frame. The full-field strain and displacement were obtained by two cameras via the DIC technique. Each camera covered half of the panel with overlap at the mid-span. The LVDT was used to confirm the deflection at the mid-span obtained by using the DIC technique. Two limit states were considered, i.e., the serviceability limit states (SLS) that represent the functional or operational use and the ultimate limit states (ULS) that represent the failure of the structure and its components. The panel was considered within the SLS when the mid-span deflection was less than the value of clear span/250 (i.e., 8 mm for the specimens in this study) [45]. The bending capacity at the SLS (M_s) and ULS (M_u) in kN·m, can be determined by using Eqs. (2) and (3) as per [45], respectively.

$$M_s = 0.5\left(P_{si} + 9.81 m_f\right) l_s + 0.125 (9.81 m_{si}) l_{si} \quad (2)$$

$$M_u = 0.5\left(P_i + 9.81 m_f\right) l_s + 0.125 (9.81 m_{si}) l_{si} \quad (3)$$

where P_{si} and P_i represent the load applied to the load frame at the SLS and ULS, respectively; l_s is the clear span of the panel; l_{si} is the mean distance between the centre lines of loading bars and the centre lines of support bars; m_f is the mass of the load frame; and m_{si} is the mass of the specimen. The characteristic bending moment capacity per meter width in kN m/m at the SLS (M_{cs}) and the ULS (M_{cu}) can be calculated for the tested speciemn by using Eqs. (4) and (5) in accordance with [45], respectively.

$$M_{cs} = \lambda M_s / \mathrm{b} \quad (4)$$

$$M_{cu} = \lambda M_u / \mathrm{b} \quad (5)$$

where λ is the reduction factor (i.e., 0.63) defined in AS 5146.2 [45] and b is the width of the panel. The requirements of M_{cu} for the 50 mm-thick wall panels and 50 mm-thick floor panels were 0.18 kN m/m and 0.21 kN m/m, respectively, as per AS 5146.3 [49].

Table 5
Experimental results of the tested specimens.

Specimen	P_s (N)	M_{cs} (kN m/m)	SMI (%)	P_u (N)	M_{cu} (kN m/m)	UMI (%)	δ_u (mm)	DI (%)
AAC_T50L	98.01	0.19	–	253.82	0.23	–	55.03	–
LGC_T50L_1	384.01	0.34	68%	1294.46	0.58	110%	81.56	48%
LGC_T50L_2	401.45	0.35	69%	1302.16	0.58	110%	79.32	44%
LGC_T50S	306.24	0.33	60%	1124.12	0.54	97%	69.51	26%
LGC_T37L	236.84	0.23	13%	1010.05	0.43	57%	71.72	30%

Note: P_s = applied load at the SLS; M_{cs} = characteristic bending capacity per meter width at the SLS; SMI = increment in M_{cs} as compared to AAC_T50L; P_u = applied load at the ULS; M_{cu} = characteristic bending capacity per meter width at the ULS; UMI = increment in M_{cu} as compared to AAC_T50L; δ_u = ultimate mid-span deflection; and DI = increment in δ_u as compared to AAC_T50L.

3. Experimental results

3.1. Material properties

The material properties of AAC and LGC are compared in Table 4. It should be noted that the data of AAC was provided by the supplier [46]. As given in Table 4, the density of LGC was 1033 kg/m^3, which was 1.3 times higher than that of AAC (i.e., 765 kg/m^3). The compressive strength, modulus of rupture and modulus of elasticity of AAC were 4.18 MPa, 0.50 MPa and 1.18 GPa, respectively. As compared to AAC, an increment of 205%, 104% and 311% in the compressive strength, modulus of rupture and modulus of elasticity was obtained by LGC, respectively. It indicated that LGC had a higher strength-to-weight ratio than AAC, which can enhance the structural performance of panels. Additionally, the 3.2 mm-diameter steel wire for AAC panel had the yielding strength of 734 MPa as provided by the supplier [46]. The yield strength of the steel wire with the diameter of 3.2 mm and 2.5 mm used to reinforce LGC panels was measured as 713 MPa with the standard deviation of 4.46 MPa and 728 MPa with the standard deviation of 5.44 MPa, respectively. The steel mesh used in LGC panels had a similar yield strength to that of AAC panel, and both met the requirement of grade 500L as per [48].

3.2. Testing results of the panel

This section presents and compares the structural performance of AAC and LGC panels under four-point bending tests. The experimental results of the testing specimens are summarized in Table 5. The bending capacity was determined by the applied load provided by the hydraulic jack, self-weight of the load frame (i.e., 20 kg) and self-weight of the panels. It is noted that the applied load P_s and P_u excluded the self-weight of the loading frame and the specimen. The effects of the thickness, reinforcement configuration and using LGC material on failure modes, cracking patterns and load–deflection behaviour of the testing specimens were discussed and analysed. In addition, the enhancement of LGC panel with respect to the bending capacity at the SLS and ULS as well as ultimate mid-span deflection was determined and compared.

3.2.1. Failure modes and crack patterns

Figs. 7 (a)–(e) show the failure modes and cracking patterns of the AAC and LGC panels. For AAC_T50L, two primary cracks initiated at the soffit of the panel. With the increase of the applied load, the cracks propagated quickly along the cross-section of the panel. Then, numerous cracks formed between the primary cracks. The panel experienced AAC crushing and shattering in the middle region of the panel and failed with a sudden collapse as shown in Fig. 7 (a). The shattering of AAC was also reported in the previous studies [15,50]. It is because AAC with porous nature had low strength, which resulted in the low ductility of reinforced AAC panels.

With respect to the LGC panels, shattering was not observed at the ULS. As shown in Figs. 7 (b) and (c), the panels LGC_T50L_1 and LGC_T50L_2 both failed in the flexural mode with cracks initiated on the bottom surface. With the increase of the applied load, the cracks propagated along the transverse direction of the panel and widened after reaching the yielding of longitudinal reinforcement. Finally, LGC_T50L panels failed with LGC crushing in the compression zone. For LGC_T50S and LGC_T37L, the development of cracks was similar to that of LGC_T50L panels. As shown in Figs. 7 (d) and (e), one primary crack and several secondary cracks initiated from the tension zone. The primary crack further propagated through the full width of the panel and widened. The panel failed with a sudden drop in the loading owing to the LGC crushing in the compression zone. It is worth noting that the rupture of the longitudinal reinforcement of LGC_T50S occurred before failure, which decreased the bending capacity and ductility of the panel at the ULS as compared to LGC_T50L panels. Figs. 8 (a)–(d) show the transverse strain field of the testing panels at the ULS. As shown, the maximum strain of AAC_T50L was 4.31% in the compressive zone, which caused the AAC shattering. The maximum strain of LGC_T50L_1, LGC_T50S and LGC_T37L was measured as 9.37 %, 7.98 % and 7.01 %, respectively. The test results demonstrated that replacing AAC with LGC as matrix material in lightweight panels led to the shift of failure mode from AAC shattering of AAC panels to flexural damage of LGC panels due to the higher strength of LGC as compared to AAC.

3.2.2. Structural behaviours of LGC panels

As presented in Fig. 9, the reinforced lightweight panels showed typical flexural behaviour under four-point bending, which can be characterized by three distinct stages including the pre-cracking stage, post-cracking stage and post-yielding stage. For stage 1 (pre-cracking), the panel behaved within the elastic phase, and the load–deflection curve showed linear relationship during this stage. This stage ended when the first crack appeared on the specimen and the applied load reached the cracking load. For stage 2 (post-cracking), the mid-span deflection increased nonlinearly with the increase of applied load due to the propagation of cracks. Multiple cracks propagated upward and widened as the applied load increased. Then, tensile force of LGC panels was mainly carried by steel mesh. This stage ended when the steel mesh reached its yielding limit. For stage 3 (post-yielding), the mid-deflection increased substantially with the increased applied load during this stage owing to the reduction of panel stiffness caused by the rapid development of cracks. After that, the applied load decreased dramatically, which indicated reaching the ultimate load-bearing capacity of the reinforced LGC panel.

The load–deflection curves of all the tested panels are presented in Fig. 10. The deflection was captured by using DIC technique. According to AS 5146.2 [45], the mid-span deflection should be less than the value of clear span/250 (i.e., 8 mm) to ensure the SLS of the panel. As observed in the zoom-in graph of Fig. 10, the applied load of the LGC panels at cracking point was higher than that of the AAC panel. It is because the modulus of rupture of LGC material was 104% higher than that of AAC material. Furthermore, the LGC panels had higher stiffness as compared to the AAC panel within the SLS, which resulted in considerably higher service loads at the SLS. For instance, the service load of LGC_T50_1, LGC_T50_2. LGC_T50S and LGC_T37L were 384.01 N, 401.45 N, 306.24 N and 236.84 N, which were 3.9, 4.1, 3.1 and 2.4 times higher than that of AAC_T50L (i.e., 98.01 N), respectively. The experimental results demonstrated that replacing AAC with LGC improved the performance

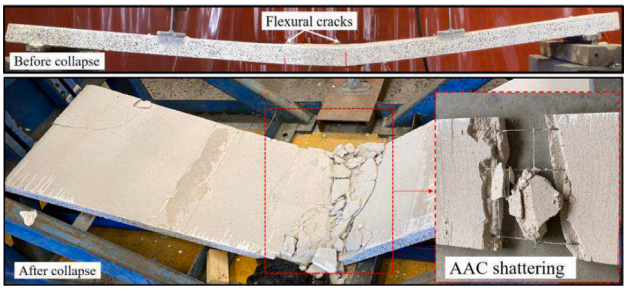

(a) AAC _T50L

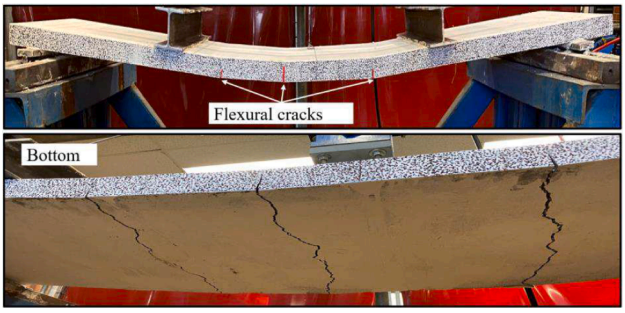

(b) LGC_T50L_1

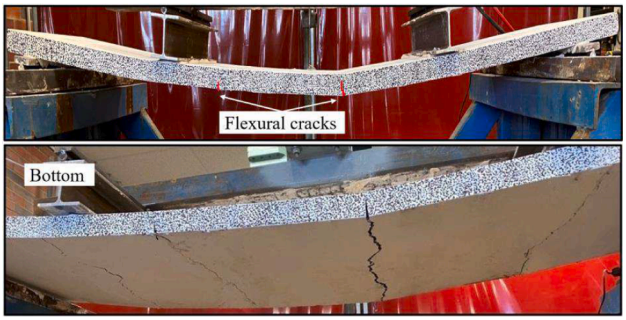

(c) LGC_T50L_2

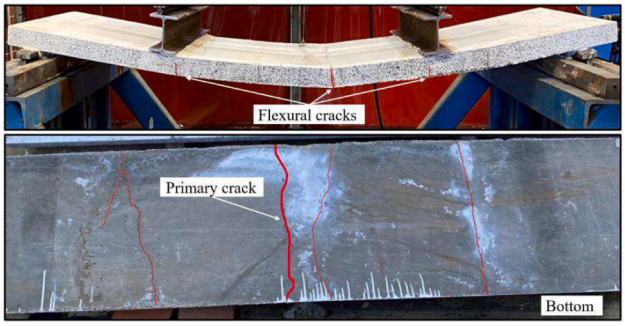

(d) LGC_T50S

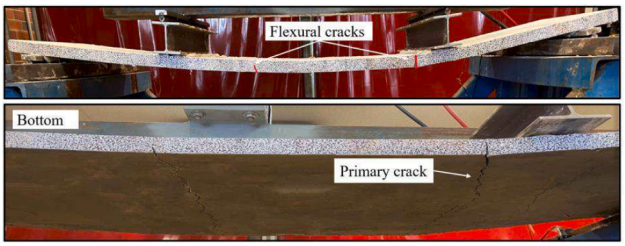

(e) LGC_T37L

Fig. 7. Failure modes and crack patterns of the tested panels.

of the panel within the SLS.

For AAC_T50L, the linear elastic behaviour was observed with the increase of the mid-span deflection at the pre-cracking stage. Then, the mid-span deflection increased nonlinearly to 4.24 mm with the applied load up to approximately 95 N because of the development of main cracks, which resulted in a sudden drop of the applied load and a remarkable reduction in stiffness. After that, numerous cracks initiated as the applied load increased, which resulted in a "saw-teeth'' increase. It should be noted that the AAC panel experienced sudden collapse at the peak load of 253.82 N with the corresponding mid-span deflection of 55.03 mm, which resulted in the failure of AAC_T50L before the yielding of longitudinal reinforcement.

As shown in Fig. 10, all the tested LGC panels showed typical flexural behaviour under four-point bending with stiffness degradation till the ultimate load. It was observed that the flexural behaviours of the two LGC_T50L panels were consistent. At first, the panels of LGC_T50L responded linearly during the pre-cracking stage. The applied load about 10% of the peak load was mainly carried by the matrix until the appearance of the crack at the cracking point. Then, the mid-span deflection increased nonlinearly to around 45 mm with the applied load up to approximately 1150 N for the post-cracking stage. During the post-cracking stage, it was observed when a new crack initiated, the applied load suddenly dropped due to the stress release, and it increased again when stress redistributed to different sections. The crack developed with the increasing applied load until the tensile stress reached the modulus of rupture of LGC. This phenomenon of the dropping loading recurred with multiple cracks developed until complete failure. Then, a substantial increase in the mid-span deflection with the slowly rising applied load was observed due to the yielding of longitudinal reinforcement. For instance, the mid-span deflection of LGC_T50L_1 increased to 81.56 mm during the post-yielding stage while the applied load increased to 1294.46 N. After that, the specimen consequently failed in flexural mode along with LGC crushing on the compression side. The mid-span deflection of LGC_T50L panels at the ULS was about 80 mm, which was 1.45 times more than that of AAC_T50L.

The load–deflection behaviour of LGC_T50S was similar to that of LGC_T50L. As observed, the applied load was 1023 N with the corresponding mid-span deflection of 37 mm at the yielding point. Then, when the mid-span deflection increased to 69.51 mm, the load reached the ultimate load of 1124.12 N with a gradual reduction in stiffness. The mid-span deflection of LGC_T50S was 26% higher than that of AAC_T50L. However, the bending capacity and mid-span deflection of LGC_T50S was lower than that of LGC_T50L panels at the ULS for which the load suddenly decreased due to the rupture of the steel wire and the LGC crushing.

LGC_T37L had the similar trend of the load–deflection curve to that of LGC panels with the thickness of 50 mm but the stiffness of LGC_T37L with 37.5 mm thickness was lower. This was attributed to the 25% thinner thickness of LGC_T37L, which has a direct influence on the initial cracking moment before the crack appeared. Several significant loading drops were also observed due to the development of cracks. As shown, the applied load was 880 N with the corresponding mid-span deflection of around 45 mm at the yielding point. After that, the peak load was 1010.05 N with the corresponding deflection of 71.72 mm. An increment of 30% in the mid-span deflection was obtained by LGC_T37L as compared to that of AAC_T50L. It is worth mentioning that better structural performance can be obtained by the LGC panel with the same weight but less thickness as compared to AAC panel. The improved loading and deformation capacity are mainly attributed to the improved mechanical properties of the LGC, which consisted of the compact geopolymer matrix and lightweight aggregates [33,43].

The characteristic bending capacities in the SLS and ULS of AAC and LGC panels are summarized in Table 5. The characteristic bending capacity per meter width of AAC_T50L at the SLS was 0.20 kN·m/m. An increment of 69%, 60% and 12% was obtained by LGC_T50L, LGC_T50S and LGC_T37L, respectively. The characteristic bending capacity per

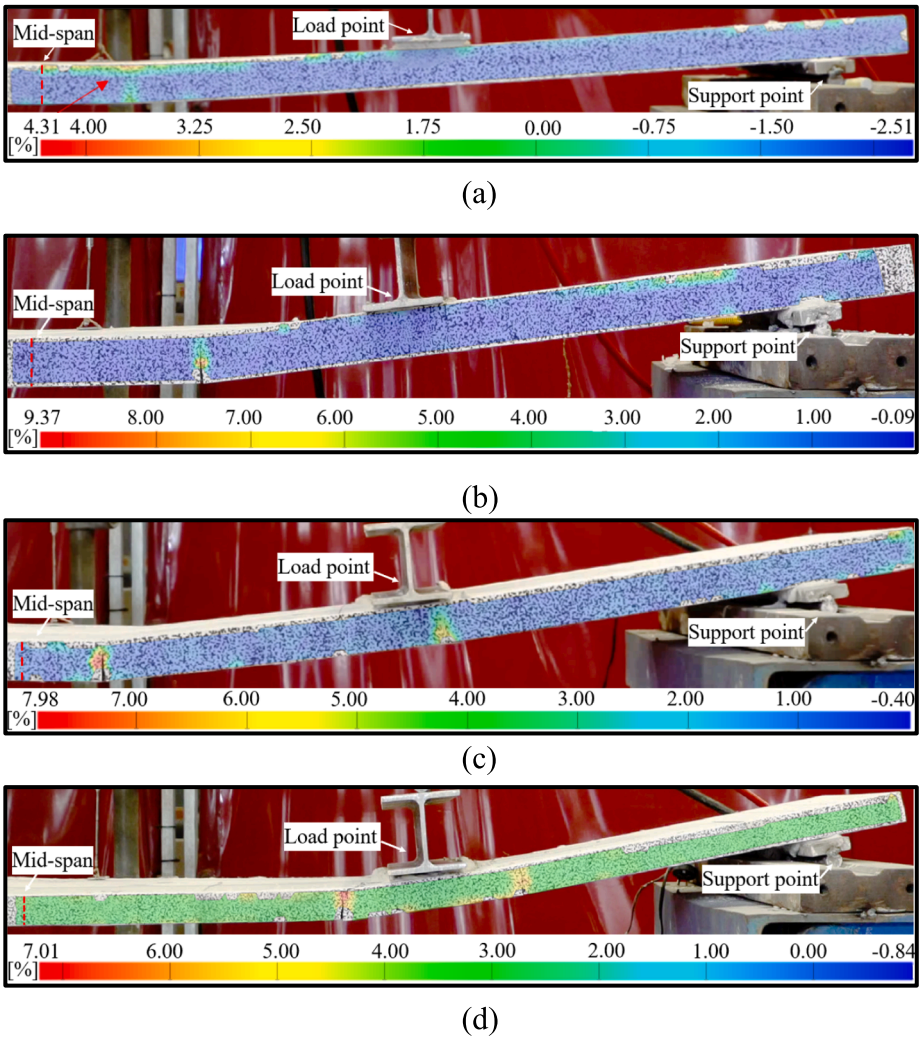

Fig. 8. Transverse strain field of the testing panels at the ULS.

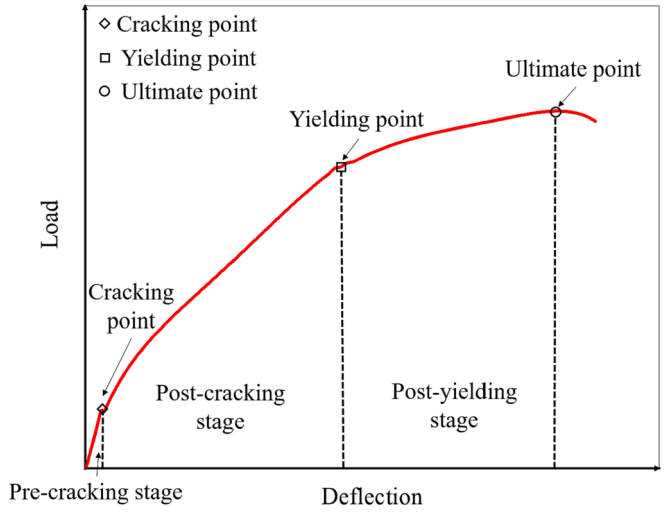

Fig. 9. Typical load–deflection curves of LGC panels.

meter width of AAC_T50L at the ULS was 0.28 kN·m/m. The characteristic ultimate bending capacity of LGC panel with the same dimension as AAC panel was around twice higher than that of AAC panel. It is worth noting that LGC_T37L had the same weight but 25% thinner than that of AAC_T50L, and a 57% higher ultimate characteristic bending capacity per meter width. The characteristic ultimate bending capacity per meter width of all the LGC panels met the requirement for the purpose of 50 mm-thick wall panels (i.e., 0.18 kN m/m) and 50 mm-thick floor panels (i.e., 0.21 kN m/m) according to AS 5146.3 [49]. In summary, the LGC panels showed much improved flexural capacity than that of AAC panel.

4. Analytical investigation

As per AS 5146.2 [45], the ultimate bending capacity (M_u) of the reinforced AAC panel can be predicted based on force equilibrium at the balanced condition. The prediction on M_u of the reinforced AAC panel is given as follows:

$$M_u = k_h \alpha (\mu_c f_c^{'}/\gamma_c) b d^2 k_n (1 - \beta k_n) \quad (6)$$

$$\alpha = 1 - (1 - k_n)\varepsilon_c/(2\varepsilon_s) \quad (7)$$

$$\beta = \{2k(1 - k_n)[-1 + 2k(1 - k_n)/3k_n] + k_n\}/[2k_n - 2k(1 - k_n)] \quad (8)$$

where k_h is the factor for the panel thickness less than 75 mm (i.e., 0.8); μ_c is the long-term reduction factor (i.e., 0.85); γ_c is the partial factor for AAC material (i.e., 1.5); f_c' is the compressive strength of AAC material; b is the width of the section; d is the effective depth from compression face to the centroid of reinforcement; k_n is the factor used to calculate the depth to the neutral axis, $k_n = \varepsilon_c/(\varepsilon_c + \varepsilon_s)$; ε_c and ε_s represent the

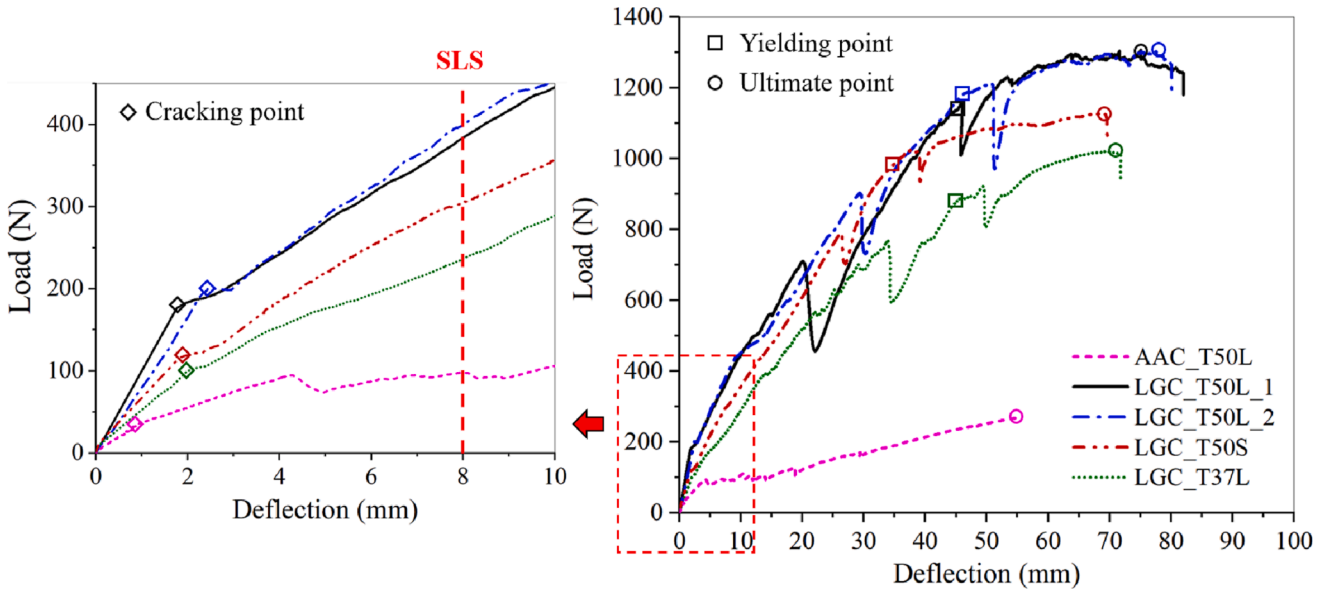

Fig. 10. Load-deflection curves of all the specimens.

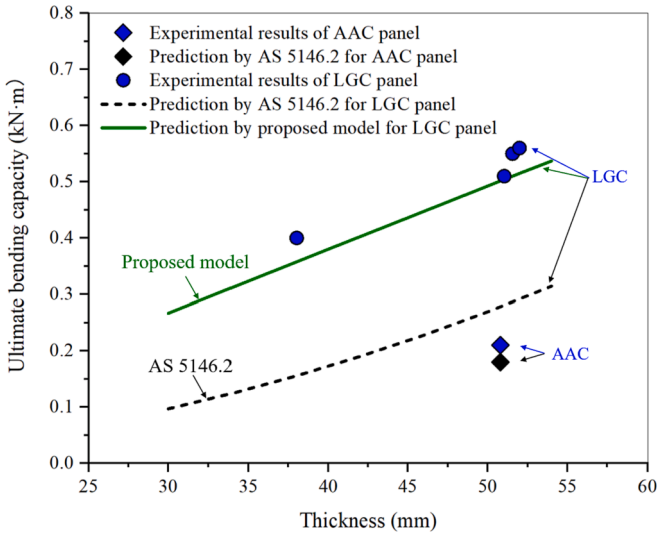

Fig. 11. Ultimate bending moment: experimental results vs analytical predictions.

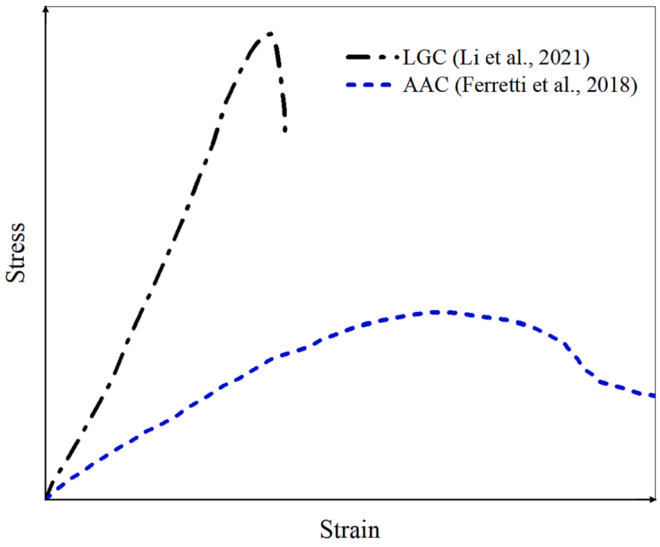

Fig. 12. Compressive stress–strain behaviours of AAC [52] and LGC [43].

strain of AAC and steel reinforcement; α is the factor defining the compressive force in the AAC, $\alpha_{max} = 0.667$; β is the factor defining the distance of the force in the AAC from the extreme compressive fibre, $\beta_{max} = 0.361$; k is the factor relating the compressive and tensile strains in bending, $k = \varepsilon_c/(3\varepsilon_s)$. The factors α and β were adopted for the stress block parameters based on the stress–strain behaviour of AAC material.

The prediction by using AS 5146.2 is compared with the experimental results as shown in Fig. 11. It was observed that AS 5146.2 can reasonably predict M_u of the AAC panel with an error margin of 13%. In addition, it was found that the model of AS 5146.2 used for AAC panels underestimated M_u of the LGC panels due to different mechanical behaviours between AAC and LGC material. Fig. 12 shows the compressive stress–strain curves of AAC and LGC material and their stress–strain curve profiles are different. LGC material shows triangular stress distribution [43] and AAC material shows parabolic stress distribution [51], which is due to the different porous structure of AAC and LGC material as shown in Fig. 13. AAC material has the fraction volume of pores from 65% to 90% [52], which was much higher than that of LGC

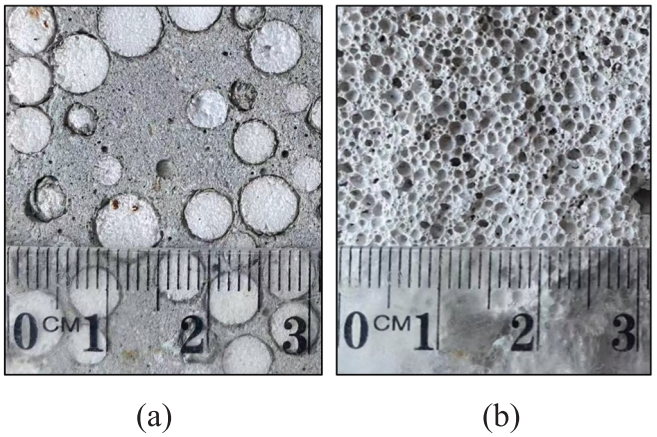

Fig. 13. Porous structure of (a) LGC and (b) AAC.

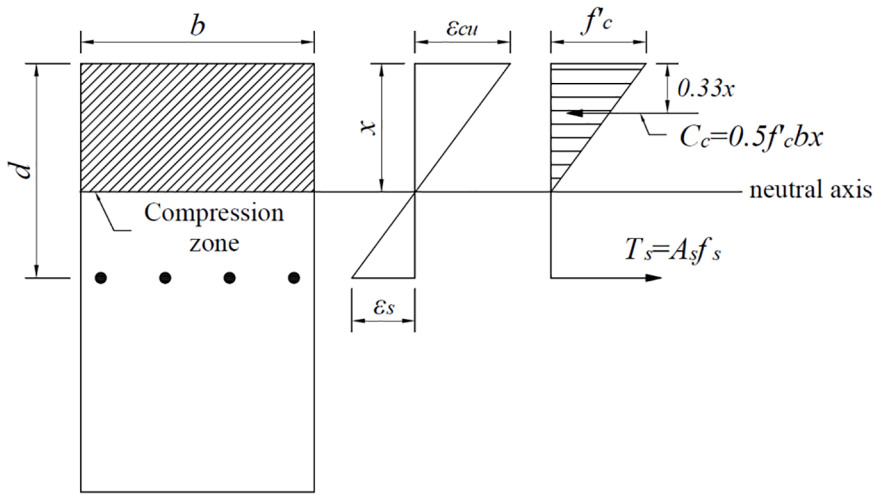

Fig. 14. Strain and stress diagram at ultimate limit state (ULS).

Table 6
Comparison of experimental and predicted ultimate bending moment of AAC and LGC panels.

Specimen	M_{exp}	M_{AS}	M_{AS}/M_{exp}	M_{pre}	M_{pre}/M_{exp}
AAC_T50L	0.21	0.18	87%	–	–
LGC_T50L_1	0.55	0.29	52%	0.51	92%
LGC_T50L_2	0.56	0.29	52%	0.51	92%
LGC_T50S	0.51	0.27	53%	0.50	97%
LGC_T37L	0.41	0.16	39%	0.37	90%

Note: M_{exp} = experimental results of the M_u; M_{AS} = predicted value of the M_u by AS 5146.2 [45]; and M_{pre} = predicted value of the M_u by the proposed model in this study.

with 30% EPS in volume. AAC experienced foam-like crushing behaviour, which was different from LGC showing more brittle behaviour. Therefore, to predict M_u of the reinforced LGC panel, an analytical model need to be developed accordingly.

The basic assumptions were adopted for the ULS analysis of LGC panel: (a) a plane cross-section remains plane after loading before yielding, (b) the concrete in tension below the neutral axis is completely cracked and tensile stress is sustained by the reinforcement only, and (c) the compressive stress of LGC was assumed distributed triangularly. Fig. 14 shows the generalized stress and strain distributions on the cross-section of the panel with a single layer of steel mesh at mid-height at the ULS. The stress block parameters α and β were determined as 0.5 and 0.33 for the triangular stress block of LGC material according to the stress distribution as shown in Fig. 14. The estimation of the ultimate bending capacity of the reinforced LGC panel was based on the equilibrium and tension-controlled section as discussed in Section 3.2.2. Therefore, the ultimate bending capacity can be calculated by using Eqs. (9) and (10).

$$M_u = 0.5 f_c^{'} bc(d - 0.33x) \tag{9}$$

$$x = 2A_s f_s / (f_c^{'} b) \tag{10}$$

where f_c' represents the compressive strength of LGC material; x is the depth to the neutral axis; A_s represents the cross-section area of reinforcement; and f_s stands for the yield strength of the reinforcement. As shown in Fig. 11, the proposed model can well predict the M_u of the reinforced LGC panel with a discrepancy of less than 10%, which is much better than the predictions by using AS 5146.2. Therefore, the proposed model can be used for the design of the developed LGC panels. The experimental and predicted results of the M_u of AAC and LGC panels are summarized in Table 6.

5. Conclusion

In this study, a new reinforced panel was developed by using lightweight geopolymer composite (LGC) for prefabricated buildings. The material properties, i.e., density, compressive strength, modulus of rupture, and modulus of elasticity of LGC and AAC were compared first. The bending responses of one AAC and four LGC panels with different thicknesses and reinforcement configurations were then investigated by conducting four-point bending tests. Based on the experimental and analytical results presented in this study, the main conclusions can be summarized as follows:

1. The density of LGC (1033 kg/m^3) was 1.3 times higher than that of AAC (765 kg/m^3), while LGC showed an increase in the compressive strength, modulus of rupture, and elastic modulus by 248%, 104%, and 311% as compared to the investigated AAC, respectively.
2. The failure modes of the panels changed from severe shattering damage of the AAC panel to flexural cracking of the LGC panels due to higher strength-to-weight ratio of LGC material.
3. The characteristic bending capacity of LGC_T50L and LGC_T50S was higher than that of AAC_T50L at the serviceability limit state (SLS) and ultimate limit states (ULS). LGC_T37L with the same weight but less thickness as compared to AAC panel obtained 12% and 57% higher bending capacity at SLS and ULS, respectively.
4. The LGC panels experienced the first crack at a much higher loading level than the AAC panel. All the panels tested in this study met the requirement of characteristic bending capacity for the applications of prefabricated cladding, walls and floors as specified in [49], indicating the potential applications of these panels made of sustainable material in construction.
5. Empirical formulae were proposed to accurately predict the ultimate bending capacity of the developed LGC panels, which can be used for design purpose.

Declaration of Competing Interest

The authors declare that they have no known competing financial interests or personal relationships that could have appeared to influence the work reported in this paper.

Acknowledgements

The authors acknowledge the financial support from the Australian Research Council (ARC) via Australian Laureate Fellowship (FL180100196).

References

[1] Hao H, Bi K, Chen W, Pham TM, Li J. Towards next generation design of sustainable, durable, multi-hazard resistant, resilient, and smart civil engineering structures. Eng Struct 2023;277:115477.
[2] Tavares V, Soares N, Raposo N, Marques P, Freire F. Prefabricated versus conventional construction: comparing life-cycle impacts of alternative structural materials. J Build Eng 2021;41:102705.
[3] Akhtar N, Ahmad T, Husain D, Majdi A, Alam MT, Husain N, et al. Ecological footprint and economic assessment of conventional and geopolymer concrete for sustainable construction. J Clean Prod 2022;134910.
[4] Hamidi F, Valizadeh A, Aslani F. The effect of scoria, perlite and crumb rubber aggregates on the fresh and mechanical properties of geopolymer concrete. Structures: Elsevier; 2022. p. 895–909.
[5] Lu L, Ding Y, Guo Y, Hao H, Ding S. Flexural performance and design method of the prefabricated RAC composite slab. Structures: Elsevier; 2022. p. 572–84.
[6] Peng L, Xiaoyong L, Ying C, Zhiwu Y, Dayou Y. Thermodynamic and acoustic behaviors of prefabricated composite wall panel. Structures: Elsevier; 2020. p. 1301–13.
[7] Ismail MK, Hassan AA, AbdelAleem BH, El-Dakhakhni W. Flexural behavior and cracking of lightweight RC beams containing coarse and fine slag aggregates. Structures: Elsevier; 2023. p. 1005–19.
[8] Devi NR, Dhir PK, Sarkar P. Influence of strain rate on the mechanical properties of autoclaved aerated concrete. J Build Eng 2022;104830.
[9] Yardim Y, Waleed AMT, Jaafar MS, Laseima S. AAC-concrete light weight precast composite floor slab. Constr Build Mater 2013;40:405–10.
[10] Wang B, Wang P, Chen Y, Zhou J, Kong X, Wu H, et al. Blast responses of CFRP strengthened autoclaved aerated cellular concrete panels. Constr Build Mater 2017; 157:226–36.
[11] Zhang G, Chen B, Miao Q, Wu H, Chen P. Experimental investigation on flexural performance of autoclaved aerated concrete slab. Proceedings of the 2014 International Conference on Mechanics and Civil Engineering. 2014.
[12] Uddin N, Fouad F, Vaidya UK, Khotpal A, Serrano-Perez JC. Structural characterization of hybrid fiber reinforced polymer (FRP) autoclave aerated concrete (AAC) panels. J Reinf Plast Compos 2016;25(9):981–99.
[13] Zhang T, Dai J, Qin S. Experimental study on shear behavior of reinforced autoclaved aerated concrete slab. J Phys Conf Ser IOP Publish 2020:012159.
[14] Jennings C, Owen NA, Tanner JE. Behavior of autoclaved aerated concrete reinforced thin-panel floor sheathing elements. ACI Struct J 2019;116(1).
[15] Wilson S, Jennings C, Tanner JE. Evaluation of exterior wall behavior using reinforced autoclaved aerated concrete as cladding. J Struct Eng 2018;144(10).
[16] Narayanan N, Ramamurthy K. Structure and properties of aerated concrete: a review. Cem Concr Compos 2000;22(5):321–9.
[17] Jos R, Lukito M. Influence of water absorption on properties of AAC and CLC lightweight concrete brick. Petra Christian University; 2011 [Doctoral dissertation]:.
[18] K. Sherin J. Saurabh Review of autoclaved aerated concrete: advantages and disadvantages Proceedings of National Conference : Advanced Structures, Materials And Methodology in Civil Engineering (ASMMCE–2018)2018. 35 39.
[19] 50 mm-thick AAC flooring system installation. https://www.kosp.com.au/aac-panel. (Accessed 10/07 2022).
[20] 50 mm-thick AAC cladding panel installation. https://www.youtube.com/watch?v=NXzGOMR7Acw. (Accessed 10/07 2022).
[21] Tayeh BA, Zeyad AM, Agwa IS, Amin M. Effect of elevated temperatures on mechanical properties of lightweight geopolymer concrete. Case Stud Constr Mater 2021;15:e00673.
[22] M.F. Junaid ur Rehman Z, Kuruc M, Medveď I, Bačinskas D, Čurpek J, et al. Lightweight concrete from a perspective of sustainable reuse of waste byproducts Construction and Building Materials. 2022;319:126061.
[23] Khan MZN, Hao Y, Hao H, Shaikh FUA. Mechanical properties of ambient cured high strength hybrid steel and synthetic fibers reinforced geopolymer composites. Cem Concr Compos 2018;85:133–52.
[24] Öztürk O. Engineering performance of reinforced lightweight geopolymer concrete beams produced by ambient curing. Struct Concr 2022;23(4):2076–87.
[25] Mousavinejad SHG, Gashti MF. Effects of alkaline solution/binder and Na2SiO3/NaOH ratios on fracture properties and ductility of ambient-cured GGBFS based heavyweight geopolymer concrete. Structures: Elsevier; 2021. p. 2118–29.
[26] Mousavinejad SHG, Sammak M. An assessment of the effect of Na2SiO3/NaOH ratio, NaOH solution concentration, and aging on the fracture properties of ultra-high-performance geopolymer concrete: The application of the work of fracture and size effect methods. Structures: Elsevier; 2022. p. 434–43.
[27] Shi J, Liu B, He Z, Liu Y, Jiang J, Xiong T, et al. A green ultra-lightweight chemically foamed concrete for building exterior: A feasibility study. J Clean Prod 2021;288:125085.
[28] Solomon AA, Hemalatha G. Characteristics of expanded polystyrene (EPS) and its impact on mechanical and thermal performance of insulated concrete form (ICF) system. Structures: Elsevier; 2020. p. 204–13.
[29] Maaroufi M, Abahri K, El Hachem C, Belarbi R. Characterization of EPS lightweight concrete microstructure by X-ray tomography with consideration of thermal variations. Constr Build Mater 2018;178:339–48.
[30] Kakali G, Kioupis D, Skaropoulou A, Tsivilis S. Lightweight geopolymer composites as structural elements with improved insulation capacity. MATEC Web Conf EDP Sci 2018:01042.
[31] Posi P, Ridtirud C, Ekvong C, Chammanee D, Janthowong K, Chindaprasirt P. Properties of lightweight high calcium fly ash geopolymer concretes containing recycled packaging foam. Constr Build Mater 2015;94:408–13.
[32] Priyanka E, Sathyan D, Mini KM. Functional and strength characteristics of EPS beads incorporated foam concrete wall panels. Mater Today: Proc 2021;46: 5167–70.
[33] Colangelo F, Roviello G, Ricciotti L, Ferrandiz-Mas V, Messina F, Ferone C, et al. Mechanical and thermal properties of lightweight geopolymer composites. Cem Concr Compos 2018;86:266–72.
[34] Qu X, Zhao X. Previous and present investigations on the components, microstructure and main properties of autoclaved aerated concrete–A review. Constr Build Mater 2017;135:505–16.
[35] Prasittisopin L, Termkhajornkit P, Kim YH. Review of concrete with expanded polystyrene (EPS): performance and environmental aspects. J Clean Prod 2022; 132919.
[36] Ouellet S, Cronin D, Worswick M. Compressive response of polymeric foams under quasi-static, medium and high strain rate conditions. Polym Test 2006;25(6): 731–43.
[37] Li Z, Chen W, Hao H, Khan MZN, Pham TM. Dynamic compressive properties of novel lightweight ambient-cured EPS geopolymer composite. Constr Build Mater 2021;273:122044.
[38] Dissanayake DMKW, Jayasinghe C, Jayasinghe MTR. A comparative embodied energy analysis of a house with recycled expanded polystyrene (EPS) based foam concrete wall panels. Energ Buildings 2017;135:85–94.
[39] Assaad J, Chakar E, Zéhil G-P. Testing and modeling the behavior of sandwich lightweight panels against wind and seismic loads. Eng Struct 2018;175:457–66.
[40] Lee J, Kang S, Ha Y, Hong S. Structural behavior of durable composite sandwich panels with high performance expanded polystyrene concrete. International Journal of Concrete Structures and Materials 2018;12(1):1–13.
[41] Amran YM, El-Zeadani M, Lee YH, Lee YY, Murali G, Feduik R. Design innovation, efficiency and applications of structural insulated panels: A review. Structure. Elsevier; 2020. p. 1358–79.
[42] Nguyen DH, Han ND, Vu AT, Nguyen TK, Hoang TN. Experimental investigation on flexural behavior of reinforced lightweight concrete slabs using recycled expanded polystyrene. Structural Health Monitoring and Engineering Structures. Springer; 2021. p. 241–50.
[43] Li Z, Chen W, Hao H, Khan MZN. Physical and mechanical properties of new lightweight ambient-cured EPS geopolymer composites. J Mater Civil Eng (ASCE) 2021;33(6):04021094.
[44] Abdel-Kader M, Fouda A. Effect of reinforcement on the response of concrete panels to impact of hard projectiles. Int J Impact Eng 2014;63:1–17.
[45] Standards Australia, Reinforced autoclaved aerated cncrete Part 2. AS 51462. North Sydney2018.
[46] WESTGYP. Nasahi External Walls. https://wwwwestgypcomau/product-category/lightweight-building-materials/ Accessed 17/03 2022.
[47] ASTM C618–19. Standard specification for coal fly ash and raw or calcined natural pozzolan for use in concrete. West Conshohocken, PA: ASTM International; 2019.
[48] Standards Australia, Steel for the reinforcement of concrete. AS 4671. North Sydney2019.
[49] Zhang G, Chen B, Wu H, Xiao W. Research on bending performance and engineering application of autoclaved aerated concrete roof panel. In: International Conference on Mechanics and Civil Engineering (ICMCE 2014): Citeseer; 2014. p. 1025–30.
[50] Ferretti D, Gherri B, Michelini E. Eco-mechanical indexes for sustainability assessment of AAC blocks. In: IOP Conference Series: Materials Science and Engineering: IOP Publishing; 2018. p. 012011.
[51] Schober G. Porosity in autoclaved aerated concrete (AAC): A review on pore structure, types of porosity, measurement methods and effects of porosity on properties. In: 5th International Conference on Autoclaved Aerated Concrete: Bydgoscsz Poland; 2011. p. 351–9.